

# Reflection Coefficient Calculation of a Structure Including a Porous Silicon Layer with Transfer Matrix Method and FDTD

Caglar Duman


**Abstract**—Porous silicon is an important material for a variety of application area such as anti-reflective coating for solar cells. Today, solar cell market is mostly dominated by silicon based solar cells. Porous silicon thin films are easy to fabricate and it is compatible with silicon technology. Designing porous silicon anti-reflective coating layers is a critical issue to enhance silicon based solar cell performance. There are several methods to calculate reflection coefficient of porous silicon thin layers. In this study, transfer matrix method and finite-difference time-domain method are used to calculate reflection coefficient of porous silicon thin layers. Because finite-difference time-domain method gives more accurate results, the results obtained with finite-difference time-domain method are used to control the results obtained with transfer matrix method. In transfer matrix method, refractive indices of the porous silicon layers are calculated with Bruggeman effective medium approximation. A slab consists of 20 nm thick porous silicon layer on a 30 nm thick silicon layer free standing in the air is considered for the simulations. Porosity of the porous silicon layer is taken as 30%, 40% and 50%. Also, the porous silicon layer is considered as consisted of random placed pores with randomly changing diameters between 12 and 18 nm. The simulation results show that increasing the porosity and the pore diameters cause more divergence of transfer matrix method and finite-difference time-domain method results. Transfer matrix method results are more reliable for longer wavelengths because the porous silicon begins to resemble a homogeneous medium. In this study, it is aimed to investigate validity limits of transfer matrix method by comparing finite-difference time-domain method results. In the literature, there are several numerical and experimental studies investigating reflection coefficient of porous silicon. But best of our knowledge, there is no study investigating dependence of reflection coefficient on both the porosity and the pore sizes of porous silicon and validity limitation of transfer matrix method in the literature.

**Index Terms**— Anti-Reflective Coating, Solar Cell, Reflection Coefficient, TMM, FDTD.

## I. INTRODUCTION

**A**BUNDANCE OF silicon in the nature and its compatibility with today's electronic technology make it

ÇAĞLAR DUMAN, is with Department of Electrical and Electronic Engineering University of Erzurum Technical University, Erzurum, Türkiye, (e-mail: [caglarduman@erzurum.edu.tr](mailto:caglarduman@erzurum.edu.tr)).

 <https://orcid.org/0000-0002-1845-8605>

Manuscript received Jul 18, 2022; accepted Oct 25, 2022.

DOI: [10.17694/bajece.1144847](https://doi.org/10.17694/bajece.1144847)

useful for a variety of applications. Porous silicon (PSi) is discovered in 1956 at Bell Labs, and it has great attention in 1990 by the scientific community with Leigh Canham's study. In following years, papers about its potential applications in microelectronics, optoelectronic devices, chemical and biological sensing are published. PSi is a sponge-like form of the silicon [1-3]. PSi is used for many applications in solar cells, fuel cells, biology, nanoenergetics, microelectromechanical systems, sensors, and photonic crystals [4]. An important feature of PSi is photoluminescence property. This property is because of excitonic recombination quantum confined in silicon nanocrystals. Although, its chemical instability, slow speed operation, disordered nature and fabrications problems are limits PSi usage for the photoluminescence applications, there are ongoing studies to overcome these problems [5]. Multilayer PSi structures are important for various areas such as optoelectronic and sensing applications. Some fabrication errors can cause significant changes optical properties of multilayer PSi structures. In a pioneer study investigating multilayer PSi structures with numerical and experimental methods, it is stated that with some basic precautions in multilayer PSi structure fabrication their optical performances can be increased [6]. In silicon thin film solar cells, layer or layers consist of PSi can be used as anti-reflective coating (ARC) which very necessary to enhance light trapping mechanism of the solar cell [2].

In [7], mathematical modeling of anti-reflective subwavelength structures is reviewed. The methods include effective medium theory (EMT), finite-difference time-domain (FDTD), transfer matrix method (TMM), the Fourier modal method (FMM)/rigorous coupled-wave analysis (RCWA) and the finite element method (FEM). All methods predict the broadband reflection of tapered nanostructures with periods smaller than the wavelengths of light of interest and lengths that are at least a large portion of the wavelengths. In [8], reflection spectra are obtained for designed nanostructure geometries on amorphous silicon thin-film solar cells, using a Ray Tracing modelling approach. This coating reduced reflectance in the wavelength of 300–800 nm range by an average of 2.665% and 11.36% at 0° and 80° incident light, respectively. A reflectance reduction of 19.192% is obtained for wavelength of 300 nm and 80° incident light.

To design ARCs consisted of PSi layer or layers, refractive index of the PSi is to be known. Bruggeman effective medium

approximation (EMA) is an effective method to calculate refractive index of the PSi but it is reliable if wavelength of incident light is much larger than the pore sizes of the PSi. If refractive index of the PSi is known by using transfer matrix method (TMM), reflection coefficient of the PSi including structure can be calculated. In the literature several studies, using TMM to analysis structures including PSi [9-11]. FDTD method also can be used to the reflection coefficient [12, 13]. While using FDTD method, knowing refractive index of the PSi is not necessarily so FDTD gives more accurate reflection coefficient results. In [14], FDTD calculation and reflectance measurement are performed for PSi with porosity equal to 60% and it is found that FDTD calculations agree with the measured reflectance. Best of our knowledge, there is no study investigating dependence of reflection coefficient both on the porosity and the pore sizes of porous silicon and validity limitation of transfer matrix method in the literature.

In the study, a two layered structure, consists of 20 nm thick PSi layer on a 30 nm thick silicon layer free standing in the air is considered. For different porosities and pore sizes, TMM and FDTD simulations are performed to observe limitation of TMM method. In the 2<sup>nd</sup> and 3<sup>rd</sup> sections of this manuscript, information about pore structure of PSi thin films and calculation of refractive index of PSi are presented, respectively. In 4<sup>th</sup> and 5<sup>th</sup> sections of the manuscript, reflection coefficient calculation with TMM and FDTD are explained. In the 6<sup>th</sup> section, the model used in simulations and obtained results are given. Finally, in the Conclusions section, the results are summarized and argued.

## II. POROUS SILICON FABRICATION

Even though, there are more than 20 methods to fabricate PSi structures, electrochemical etching is the most preferred method to fabricate PSi structures because it is simple and economical. This method is performed in hydrofluoric (HF) solution but just dipping the silicon in HF is not formed PSi. A current flow between two electrodes, which is the silicon at the anode and platinum at the cathode is needed [3, 15]. In electrochemical etching, current density, HF concentration, temperature, etching time, type of silicon and dopant concentration are the parameters effecting formation of the pores [16].

There are ongoing debates about exact pore formation mechanism [4]. But there are studies in the literature showing selective pore direction is <100>. For (001) oriented silicon substrates, there is only one <100> direction which is perpendicular to the surface thus the pores form in well-defined columnar structure [17]. From TEM images of such PSi layers it is seen that it is possible to obtain pores with smooth walls and homogeneous thicknesses without inter connections between the pores [3]. In this study, the pores are considered as randomly distributed cylindrical structures perpendicular to the surface with smooth walls. Because of their random distribution they can overlap with each other and form a more complex pattern.

## III. REFRACTIVE INDEX OF POROUS SILICON

Porosity of a PSi wafer is show air volume in the structure and determined as in Equation 1 [1].

$$P = \frac{m_1 - m_2}{m_1 - m_3} \quad (1),$$

where P is the porosity,  $m_1$ ,  $m_2$  and  $m_3$  are the results from weight measurements before the anodic reaction, after the anodic reaction and finally after dissolution of the porous material in a molar acidic aqueous solution, respectively. Pores in a PSi are randomly arranged and the PSi can be group according to pore sizes. If the pore sizes are less than 4 nm it named as nanoporous silicon and if the pore sizes are in the range of 4 – 50 nm it named as mesoporous silicon [14]. By using Bruggeman EMA, refractive index of the PSi can be determined. EMA approximation is acceptable while wavelength of the incidence light is much larger than the pore sizes. Under this condition, the incident light does not distinguish the silicon and the void (air) and the PSi can be considered as a homogeneous medium. From Bruggeman EMA, the dielectric constant of a PSi layer can be determined as in Equation 2 [1, 18].

$$(1 - P) \left( \frac{\epsilon_{r,Si} - \epsilon_{r,eff}}{\epsilon_{r,Si} + (d - 1)\epsilon_{r,eff}} \right) + P \left( \frac{\epsilon_{r,air} - \epsilon_{r,eff}}{\epsilon_{r,air} + (d - 1)\epsilon_{r,eff}} \right) = 0 \quad (2),$$

where  $\epsilon_{r,Si}$ ,  $\epsilon_{r,eff}$ , and  $\epsilon_{r,air}$  are the dielectric constants of silicon, PSi and air, respectively. In Equation 2,  $d$  is the system dimensionality and it is 3 for the nanoporous silicon and 2 for the mesoporous silicon [18]. The calculated effective dielectric constant ( $\epsilon_{r,eff}$ ) can be used to determine complex refractive index of the PSi ( $\tilde{n}$ ) by using equality of  $\epsilon_{r,eff} = \tilde{n}^2$ . By using Equation 2, refractive index variation with porosity of a nanoporous silicon and mesoporous silicon is obtained as shown in Figure 1.

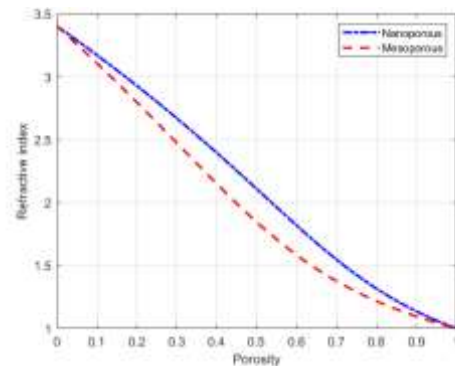


Figure 1. Refractive index variation with porosity for nanoporous silicon and mesoporous silicon.

It is seen from Figure 1, refractive index of the PSi varies between refractive index of silicon which is taken as 3.4 and refractive index of the air and with it is decrease with increasing of the porosity, as expected.

IV. REFLECTION COEFFICIENT CALCULATION WITH TMM

After calculating the refractive index, reflection coefficient of the layers composed of a PSi layer and a silicon layer can be calculated. For the calculation, transfer matrix of the structure is generated as in Equation 3 [19].

$$T_l = \begin{bmatrix} (1+p_l)e^{-i\tilde{n}_l d_l \omega/c} & (1-p_l)e^{-i\tilde{n}_l d_l \omega/c} \\ (1-p_l)e^{+i\tilde{n}_l d_l \omega/c} & (1+p_l)e^{+i\tilde{n}_l d_l \omega/c} \end{bmatrix} \quad (3).$$

In Equation 3,  $\tilde{n}_l = n_l \cos \theta$  where  $n_l$  is refractive index of the  $l^{th}$  layer and  $\theta$  is the angle of incidence. Also,  $d_l$ ,  $\omega$  and  $c$  show thickness of the  $l^{th}$  layer, radial frequency of the incident wave and speed of light, respectively. Finally,  $p_l$  is expressed as in Equation (4).

$$p_l(\omega) = \begin{cases} \frac{\tilde{n}_{l-1}}{\tilde{n}_l} & \text{for TE waves} \\ \frac{\tilde{n}_{l-1}^2 n_l^2}{\tilde{n}_l n_{l-1}^2} & \text{for TM waves} \end{cases} \quad (4).$$

The overall transfer matrix is obtained by sequentially multiplying the transfer matrices. The obtained transfer matrix can be considered as in Equation (5).

$$T = \begin{bmatrix} a & b \\ b^* & a^* \end{bmatrix} \quad (5),$$

where  $*$  is denotes the complex conjugate. Reflection coefficient of the structure is given as in Equation (6).

$$\Gamma = -\frac{b^*}{a} \quad (6).$$

V. REFLECTION COEFFICIENT CALCULATION WITH FDTD METHOD

FDTD method is first described by Yee in 1966. It solves time dependent Maxwell’s equations by approximating time and space as finite differences. FDTD method can be used for solving electromagnetic problems involving arbitrary geometries with no approximations other than curved structures modelled with a stair step approximation which cause errors [20, 21]. Also, FDTD method needs great computation power and time but it can simulate electromagnetic waves interaction with actual geometries more accurately [8].

For calculating reflection coefficient of a slab, a technique that integrating sources far from the problem zone into the FDTD method can be used. This method is known as scattered field formulation. Far-zone sources generate the incident fields outside the FDTD problem space and so there are no scatterers.

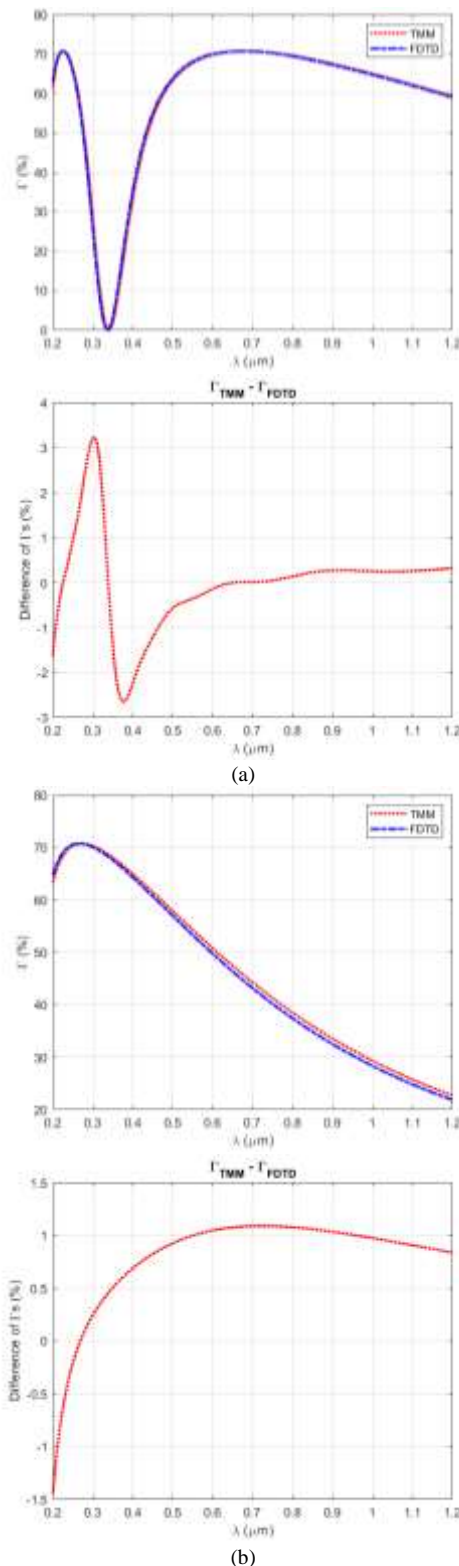


Figure 2. Reflection coefficients and their differences for porosity of a) 0% and b) 100%.

The field in the FDTD problem space is called total field and it is sum of the incident field and the scattering field. By rearranging FDTD equations accordingly, the scattered field and the incident field can be calculated while the simulation is running. The reflected field from the slab is the scattered field, and the ratio of the reflected field to incident field is the

reflection coefficient as shown in Equation 7 [19].

$$|\Gamma| = \frac{|\vec{E}_{scat}|}{|\vec{E}_{inc}|} \quad (7).$$

For a slab including P*Si* layer, the scattered field should be sampled at a surface below the slab, and the incident field should be sampled at the same surface. In this study, 3D FDTD calculation with CPML boundaries are applied and detailed explanation of the FDTD calculations is as in [22].

VI. MODEL AND SIMULATION RESULTS

In the study, a slab consists of 20 nm thick P*Si* layer on a 30 nm thick silicon layer free standing in the air is considered. Porosity of the P*Si* layer is taken as 30%, 40% and 50% and the refractive indices for these porosities is calculated with Bruggeman EMA. For FDTD simulation a slab with same thickness is considered. It is assumed that the slab is lies in the xy plane by penetrating into the CPML boundaries for 16 cells long in positive and negative x and y directions. 10 cells long air buffer and 16 cells long CPML layer are placed in positive and negative z boundaries. The width and length of the slab are 80 nm.

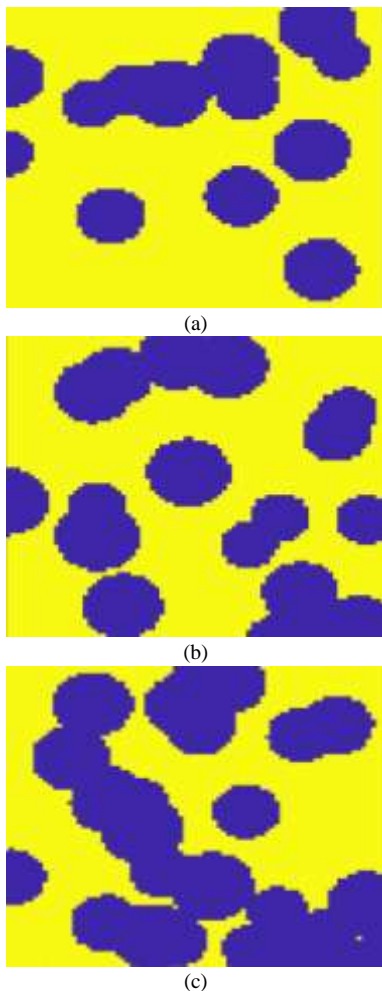
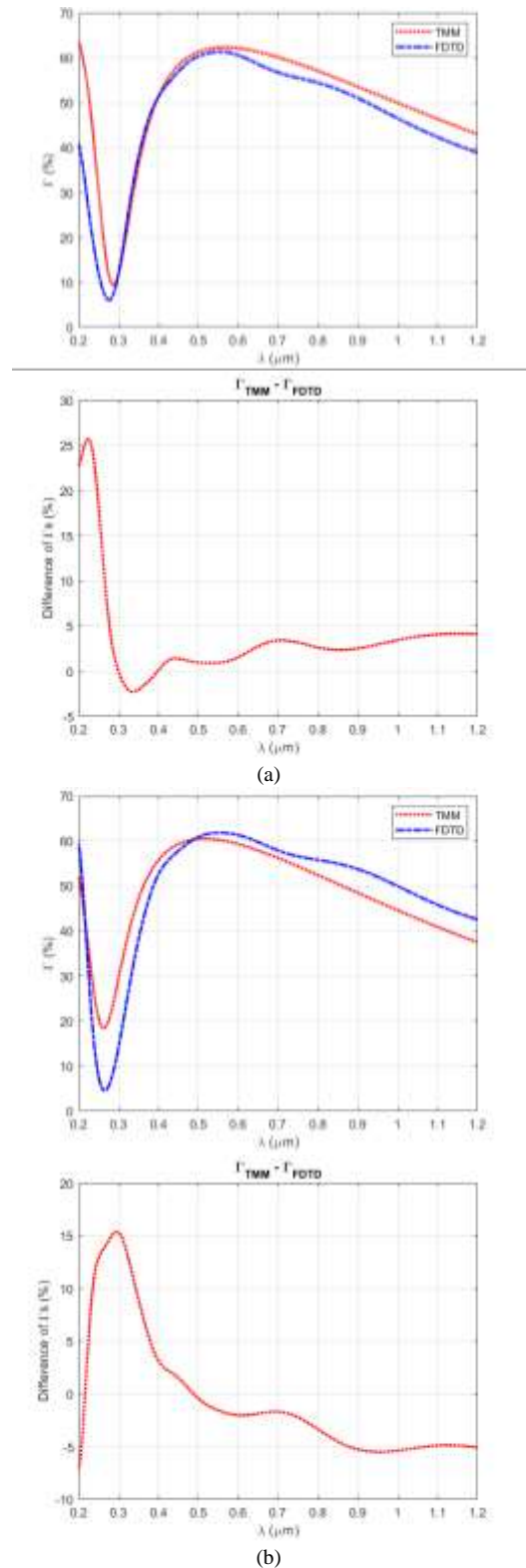


Figure 3. Obtained P*Si* layers for porosities of (a) 30%, (b) 40% and (c) 50%.



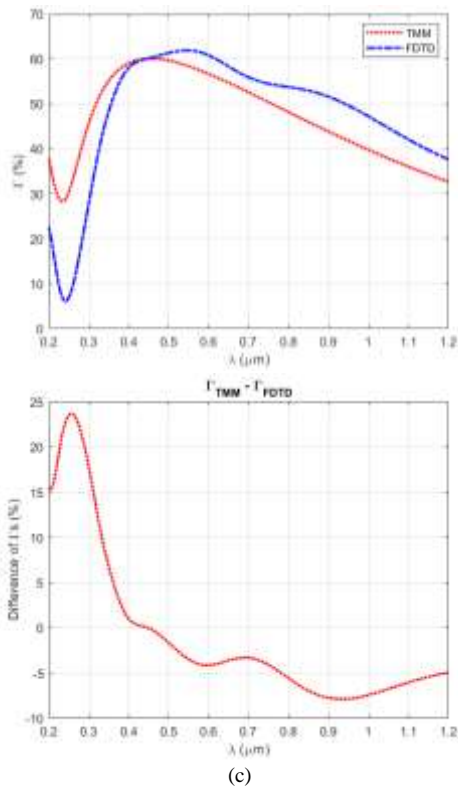


Figure 4. Obtained reflection coefficient and their differences for PSi layers with porosities of (a) 30%, (b) 40% and (c) 50%.

The incident light is x-polarized derivative gaussian shaped planar wave travelling in positive z direction. The scattered and incident fields are sampled at a surface 5 cells below the FDTD problem space. To test FDTD program, the reflection coefficient with FDTD and TMM are calculated for 0% porosity and %100 porosity. Porosity of 0% means no void in the PSi layer and porosity of 100% means no PSi layer. The results are shown in Figure 2.

It is seen from Figure 2-a and -b, the results obtained with TMM and FDTD methods well agrees but there are small differences because of the numerical errors which occur in the FDTD method. By reducing the spatial step size and the simulation time the results can be improved. In FDTD simulations, the PSi layer is created by random placed pores with randomly changing diameters between 12 and 18 nm and it is considered that the pores are perfectly continuous until the end of the PSi layer. The number of pores and their sizes are adjusted so as to reach the desired porosity. Obtained PSi layers for porosities of 30%, 40% and 50% are as shown in Figure 3.

In Figure 3, silicon portion of the PSi is shown with yellow and air portion of the PSi is shown with blue. Obtained reflection coefficient for PSi layers with porosities of 30%, 40% and 50% are shown in Figure 4.

It is seen from the figure, with increasing porosity the differences of the obtained reflection coefficients are also increase. Moreover, the results are more similar at high wavelengths and the differences decrease with increasing wavelength. The results obtained by using TMM is become more accurate at higher wavelengths because EMA approximation is acceptable while wavelength of the incidence

light is much larger than the pore sizes. Under this condition, the incident light does not distinguish the silicon and the void (air) and the PSi can be considered as a homogeneous medium [1]. To observe effect of pore distribution on FDTD simulations, second set of PSi layers with same porosities are considered. Distribution of the pores are different from previous PSi layers because of their random nature. Obtained PSi layers are shown in Figure 5.

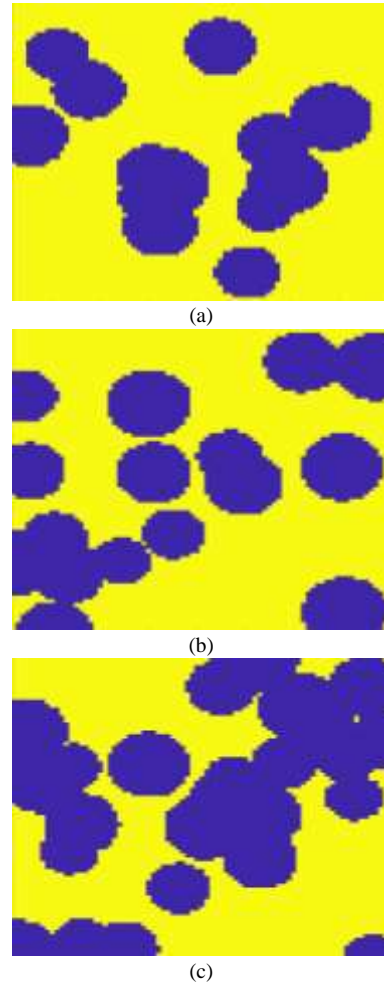
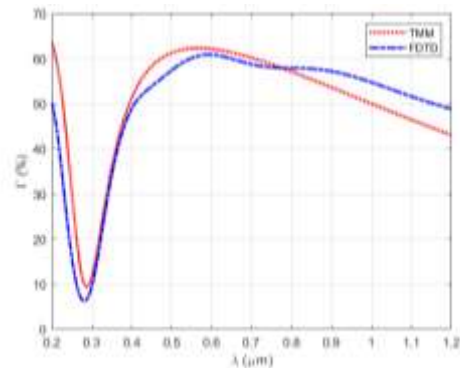
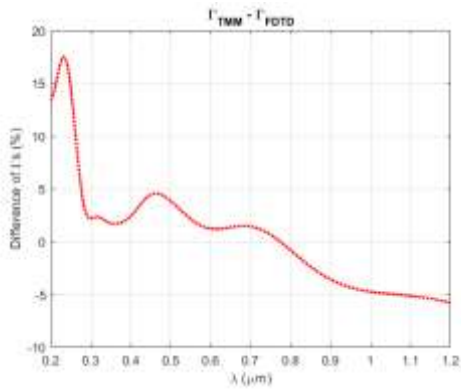


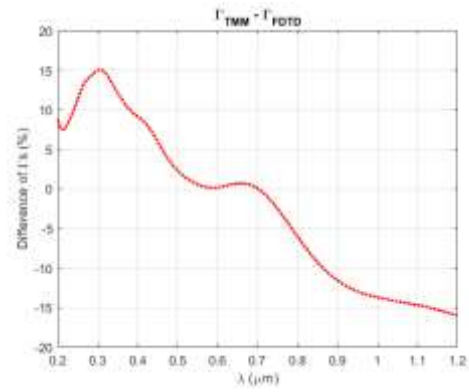
Figure 5. Second set of PSi layers for porosities of (a) 30%, (b) 40% and (c) 50%.

Obtained reflection coefficient of PSi layers with porosities of 30%, 40% and 50% are as in Figure 6.



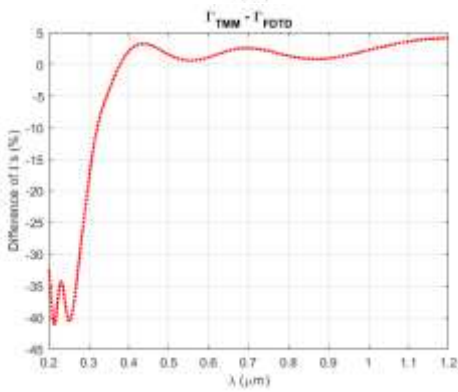
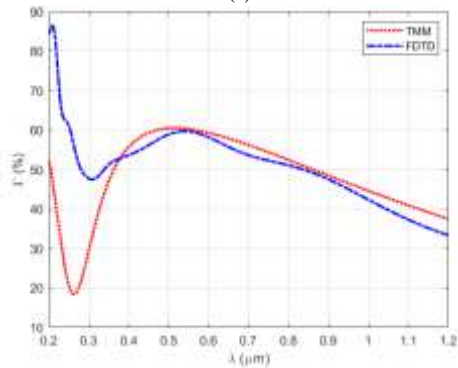


(a)

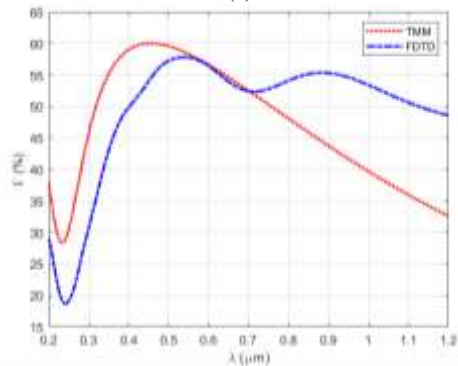


(c)

Figure 6. Obtained reflection coefficient of PSi layers and their differences with porosities of (a) 30%, (b) 40% and (c) 50%.



(b)



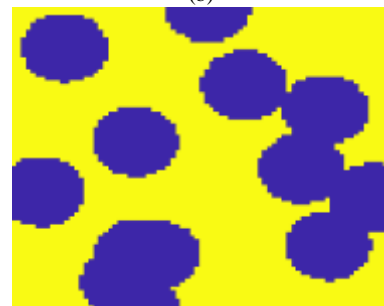
Even though results shown in Figure 6 are different from results shown in Figure 4, they show similar variations. The pore sizes are fixed 12 nm, 15 nm and 18 nm for 40% porosity and effect of pore size is evaluated. Obtained PSi layers can be seen in Figure 7.



(a)



(b)



(c)

Figure 7. Obtained PSi layers with 40% porosity for pore diameters are (a) 12 nm (b) 15 nm and (c) 18 nm.

Obtained reflection coefficient of PSi layers with 40% porosity for pore diameters are 12 nm, 15 nm and 18 nm are as

in Figure 8.

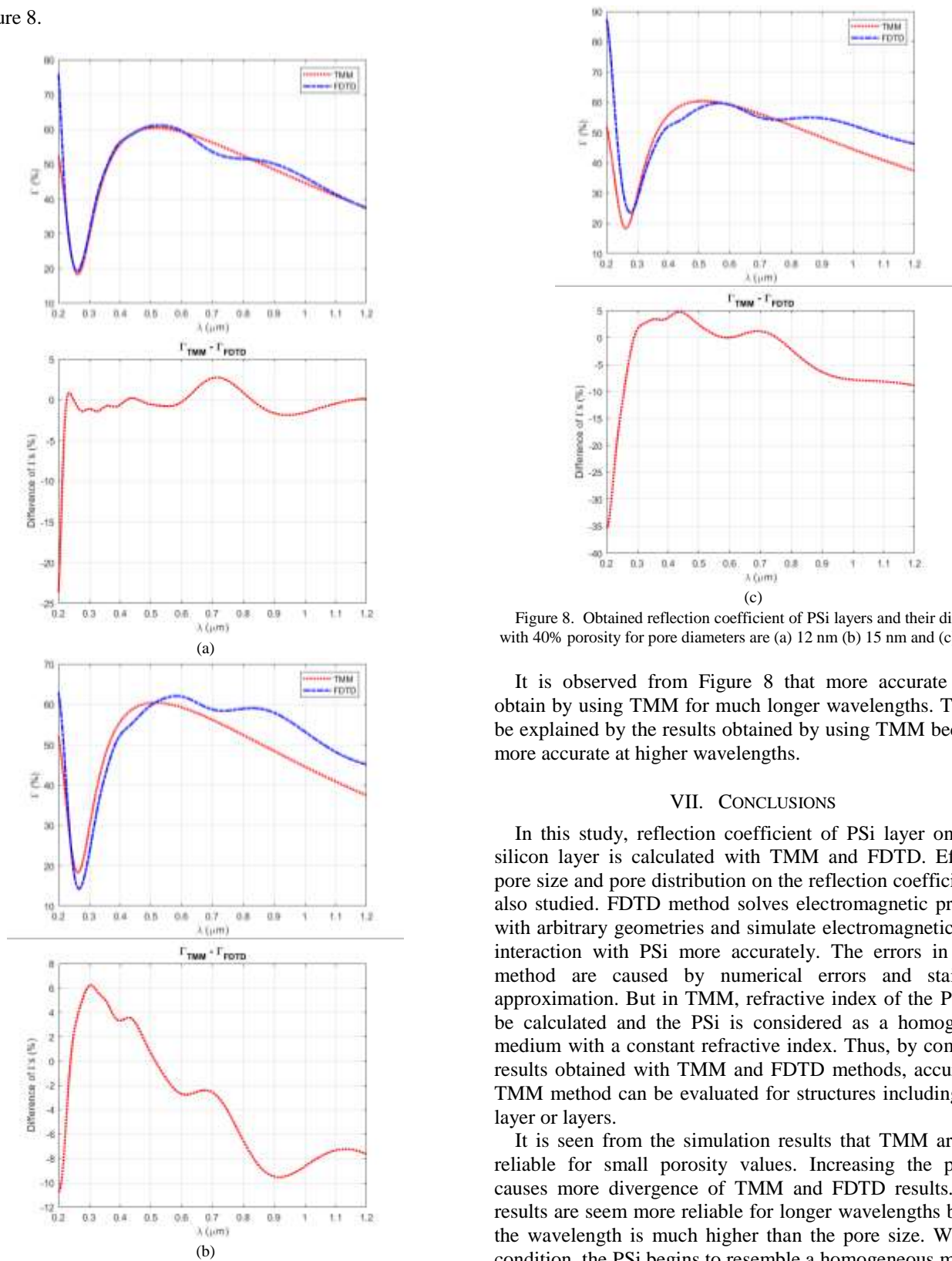


Figure 8. Obtained reflection coefficient of PSi layers and their differences with 40% porosity for pore diameters are (a) 12 nm (b) 15 nm and (c) 18 nm.

It is observed from Figure 8 that more accurate results obtain by using TMM for much longer wavelengths. This can be explained by the results obtained by using TMM becoming more accurate at higher wavelengths.

## VII. CONCLUSIONS

In this study, reflection coefficient of PSi layer on a thin silicon layer is calculated with TMM and FDTD. Effect of pore size and pore distribution on the reflection coefficient are also studied. FDTD method solves electromagnetic problems with arbitrary geometries and simulate electromagnetic waves interaction with PSi more accurately. The errors in FDTD method are caused by numerical errors and stair step approximation. But in TMM, refractive index of the PSi is to be calculated and the PSi is considered as a homogeneous medium with a constant refractive index. Thus, by comparing results obtained with TMM and FDTD methods, accuracy of TMM method can be evaluated for structures including a PSi layer or layers.

It is seen from the simulation results that TMM are more reliable for small porosity values. Increasing the porosity causes more divergence of TMM and FDTD results. TMM results are seem more reliable for longer wavelengths because the wavelength is much higher than the pore size. With this condition, the PSi begins to resemble a homogeneous medium. In addition, since the pore size and pore distribution of PSi are random, the reflection coefficient vary depending on the PSi layer on which the calculations are made. However, since the refractive index of the medium is considered as constant in TMM, this can only be observed from the FDTD results.

The analyzes carried out in this study show that PSi ARC

analysis made by using TMM will be reliable if wavelength of the incident light is much higher than the pore sizes. To obtain reliable results at lower wavelengths FDTD method should be preferred. The results are also important for practical applications. By using optical analysis during design phase of a practical application, expensive reworks can be avoided. At the design phase, if TMM with EMA would be used, porosity of the PSi should be low and pore sizes of the PSi should be smaller than interested wavelength range. Otherwise, methods such as FDTD should be used to obtain realistic results.

## REFERENCES

- [1] Basu, S. (Ed.). (2011). Crystalline Silicon: Properties and Uses. BoD-Books on Demand.
- [2] Dubey, R. S., & Gautam, D. K. (2011). Porous silicon layers prepared by electrochemical etching for application in silicon thin film solar cells. *Superlattices and Microstructures*, 50(3), 269-276.
- [3] Karbassian, F. (2018). Porous silicon. In *Porosity-Process, Technologies and Applications*. IntechOpen.
- [4] Zhao, M., Balachandran, R., Allred, J., & Keswani, M. (2015). Synthesis of porous silicon through interfacial reactions and measurement of its electrochemical response using cyclic voltammetry. *RSC advances*, 5(96), 79157-79163.
- [5] Bisi, O., Ossicini, S., & Pavese, L. (2000). Porous silicon: a quantum sponge structure for silicon based optoelectronics. *Surface Science Reports*, 38(1-3), 1-126.
- [6] Hasar, U. C., Özbek, İ. Y., & Karacalı, T. (2017). Optical Characterization of Porous Silicon Multilayers. *Handbook of Porous Silicon*, Editor: Canham Leigh, Springer, 1-12.
- [7] Han, K., & Chang, C. H. (2014). Numerical modeling of sub-wavelength anti-reflective structures for solar module applications. *Nanomaterials*, 4(1), 87-128.
- [8] Pickering, T., Shanks, K., & Sundaram, S. (2021). Modelling technique and analysis of porous anti-reflective coatings for reducing wide angle reflectance of thin-film solar cells. *Journal of Optics*, 23(2), 025901.
- [9] Wilkins, M. M., Boucherif, A., Beal, R., Haysom, J. E., Wheeldon, J. F., Aimez, V., ... & Hinzer, K. (2013). Multijunction solar cell designs using silicon bottom subcell and porous silicon compliant membrane. *IEEE Journal of Photovoltaics*, 3(3), 1125-1131.
- [10] Ariza-Flores, D., Pérez-Huerta, J. S., Kumar, Y., Encinas, A., & Agarwal, V. (2014). Design and optimization of antireflecting coatings from nanostructured porous silicon dielectric multilayers. *Solar energy materials and solar cells*, 123, 144-149.
- [11] Jimenez-Vivanco, M. R., García, G., Carrillo, J., Morales-Morales, F., Coyopol, A., Gracia, M., ... & Lugo, J. E. (2020). Porous Si-SiO<sub>2</sub> UV Microcavities to modulate the responsivity of a broadband photodetector. *Nanomaterials*, 10(2), 222.
- [12] Deinega, A. V., Konistyapina, I. V., Bogdanova, M. V., Valuev, I. A., Lozovik, Y. E., & Potapkin, B. V. (2010). Optimization of an anti-reflective layer of solar panels based on ab initio calculations. *Russian Physics Journal*, 52(11), 1128.
- [13] Min-Dianey, K. A. A., Zhang, H. C., Brohi, A. A., Yu, H., & Xia, X. (2018). Optical spectra of composite silver-porous silicon (Ag-pSi) nanostructure based periodical lattice. *Superlattices and Microstructures*, 115, 168-176.
- [14] Najjar, A., Al-Jabr, A. A., Slimane, A. B., Alsunaidi, M. A., Ng, T. K., Ooi, B. S., ... & Anjum, D. H. (2013, April). Effective antireflection properties of porous silicon nanowires for photovoltaic applications. In *2013 Saudi International Electronics, Communications and Photonics Conference* (pp. 1-4). IEEE.
- [15] Burham, N., Hamzah, A. A., & Majlis, B. Y. (2017). Self-adjusting electrochemical etching technique for producing nanoporous silicon membrane. *New Research on Silicon-Structure, Properties, Technology*.
- [16] Yaakob, S., Bakar, M. A., Ismail, J., Bakar, N. H. H. A., & Ibrahim, K. (2012). The formation and morphology of highly doped N-type porous silicon: effect of short etching time at high current density and evidence of simultaneous chemical and electrochemical dissolutions. *J. Phys. Sci*, 23(2), 17-31.
- [17] Vázsonyi, É., Battistig, G., Horváth, Z. E., Fried, M., Kádár, G., Pászti, F., ... & Poortmans, J. (2000). Pore Propagation Directions in P+ Porous Silicon. *Journal of Porous Materials*, 7(1), 57-61.
- [18] Khardani, M., Bouaicha, M., & Bessaïs, B. (2007). Bruggeman effective medium approach for modelling optical properties of porous silicon: comparison with experiment. *Physica Status Solidi c*, 4(6), 1986-1990.
- [19] Birge, J. R., & Kärtner, F. X. (2006). Efficient analytic computation of dispersion from multilayer structures. *Applied Optics*, 45(7), 1478-1483.
- [20] Pérez, E. X. (2008). Design, fabrication and characterization of porous silicon multilayer optical devices. *Universitat Rovira i Virgili*.
- [21] Hossain, M. F., & Noushin, T. (2016, December). Sensitivity enhancement of porous silicon waveguide sensor using graphene by FDTD with Lumerical software. In *2016 2nd International Conference on Electrical, Computer & Telecommunication Engineering (ICECTE)* (pp. 1-4). IEEE.
- [22] Elsherbini, A. Z., & Demir, V. (2009). The finite-difference time-domain method for electromagnetics with MATLAB simulations. Raleigh, NC: SciTech Pub.

## BIOGRAPHIES



ÇAĞLAR DUMAN was born Erzurum, in 1981. He received the B.S. and M.S. degrees in electronic engineering from the Niğde Ömer Halisdemir University in 2005 and Ataturk University in 2008, respectively, and the Ph.D. degree in electronic engineering from Ataturk University, Erzurum in 2014. Since 2014, he has been Assistant Professor in Department of Electrical and Electronic Engineering University of Erzurum Technical University. His research interests include lasers and photovoltaics.